Structure design and experimental study on ultrasonic vibration-assisted induction brazing cubic boron nitride abrasive tools

Kaida Cai
Biao Zhao (zhaobiao@nuaa.edu.cn)
Nanjing University of Aeronautics and Astronautics https://orcid.org/0000-0002-8625-3935
Bangfu Wu
Wenfeng Ding
Yanjun Zhao
Jianhui Zhu
Wenyuan Si

Research Article

Keywords: Ultrasonic vibration-assisted induction brazing device, Abrasive tools, Bonding strength, Grain morphology

Posted Date: June 23rd, 2022

DOI: https://doi.org/10.21203/rs.3.rs-1747135/v1

Abstract

Brazed abrasive tool has been widely used in high-precision machining of difficult-to-cut materials to improve the machining efficiency and quality. However, the severe wear and associated short service life during machining processes have to be faced for conventional induction brazed (CIB) abrasive tools owing to its weak bonding strength between abrasive grains and metal-bonded materials. In this case, a novel ultrasonic vibration-assisted induction brazing (UVAIB) device was developed to improve the abrasive bonding strength. Here, the frequency equation of the UVAIB device was derived using recursive methods, and then the geometric designation parameters were optimized with the finite element simulating method. In addition, the performance of UVAIB device was tested in terms of the impedance and amplitude. Subsequently, the comparative experiment trials were performed with the brazed abrasive tools under the CIB and UVAIB method. Results show that the ultrasonic energy loss of UVAIB device could be reduced, and then the amplification value and vibration uniformity could reach 8 and 92%, respectively. In addition, for CIB, there are a large number of pores and macro-cracks on the joints. However, the internal pores inside the metallic matrix of UVAIB were reduced, and only fewer and smaller micro-cracks could be found. Furthermore, the intergranular fracture of abrasive grains could be observed for CIB abrasive tools owing to the weak bonding interface caused by the existence of numerous micropores, whereas the grain transgranular fracture appeared once adopting the ultrasonic vibrating method.

1. Introduction

Brazed abrasive tool has attracted the increasing attentions in the field of aerospace industry owing to its extraordinary properties such as the high bonding strength, large chip holding space and good self-sharpening ability [1–3]. Therefore, the brazed abrasive tool has broad application in grinding of ductile material [4, 5], and the hard-brittle materials [6, 7]. However, there are still some problems with induction brazed abrasive tools. Owing to the mismatch between the mechanical and physical properties of ductile filler alloy and brittle abrasive grains, the thick connection interface constituted of loose reaction products may cause the mechanical weakening of the brazed joint, which will deteriorate the grinding performance of abrasive tools [8, 9]. Micro-cracks inevitably developed in the interface between the abrasive grains and filler alloy will also reduce the bonding strength of filler alloy on abrasive grains [10]. Therefore, effective measures need to be taken to solve the existing problems and fully develop the great potential of brazed abrasive tools. It can be considered to introduce ultrasonic into the brazing process to improve the bonding strength of the brazed joint. However, this requires the support of the UVAIB device.

Ultrasonic vibrating device has been widely used during grinding [11–13], cutting [14–16], milling [17, 18], etc. Meanwhile, in order to achieve better machining quality, various ultrasonic-assisted vibration devices have been developed. Cao et al. [19] designed a novel ultrasonic vibration plate sonotrode. The ultrasonic vibration amplitude is 7.6 μm and the plate vibration uniformity could be 95%. The grinding experiment indicated that the normal and tangential grinding forces decreased by 35% and 39%, respectively, and an improved machined surface was obtained. Zhao et al. [20] designed an ultrasonic elliptical vibration-

assisted grinding device by means of the integrated nonresonant. The experiment of grinding Nano-ZrO_2 ceramics shows that the grinding mechanism has been changed and the generation of grinding defects has been reduced. Bai et al. [21] put forward an ultrasonic elliptical vibration cutting device, which was used for ultra-precision cutting. and the results of cutting pure iron showed that the mirror surface can be achieved with almost no tool wear. Du et al. [22] proposed a piezoelectric ultrasonic milling tool with longitudinal and bending vibration achieving 39.3% cutting force reduction compared with conventional milling. However, there is currently insufficient research on the UVAIB device.

At present, ultrasonic vibration-assisted brazing technology has made beneficial progress in various materials connections. Wu et al. [23] studied the effect of ultrasonic vibration on Al/steel TIG welding-brazing joint. It was found that after ultrasonic vibration treatment, the spheroidization of the Al-Si eutectic, fragmentation of Al_3FeSi, and refinement of the aluminum matrix occurred. In addition, compared with the raw joint, the shear strength of the ultrasonic treated joint was 41 MPa higher. In fact, the effects of cavitation and acoustic streaming of ultrasonic can promote the chemical metallurgical process of liquid filler alloy during brazing [24]. Ultrasonic vibration-assisted brazing can also effectively improve the wettability of materials, so various ceramics are especially suitable for joining in this way [25, 26]. Chen et al. [27] ultrasonic vibration-assisted brazed SiC ceramic samples with ZnAlMg alloys and it was found that the duration time of ultrasonic vibration has a significant impact on the strength of the joint. When the duration time increased to 8 s, the strength of joint can reach 148 MPa. Huang et al. [28] manufactured diamond end wheel with the method of ultrasonic vibration-assisted induction brazing. As a result, the shear strength of joints increased by 28.5%, and the fracture failure of joints was greatly reduced. However, it has not been found that using UVAIB technology to manufacture abrasive tools with abrasive grains attached on the side of substrate, which can be used to grind the side of the workpiece.

The primary goal of this article is to design a novel UVAIB device, which can be used to manufacture high performance abrasive tools, and analyze the influences of ultrasonic acoustic effect on the surface morphology and abrasive bonding strength of brazing joint. Section 2 introduces the experimental setup of UVAIB. Section 3 establishes the frequency equation of the UVAIB device, conducts geometric parameter design and optimization, and tests the performance of the UVAIB device, including impedance and amplitude. Section 4 conducts a comparative investigation on CIB and UVAIB results to verify the advantages of applying ultrasonic when brazing.

2. Experimental Details

2.1 Operation method of the UVAIB device

The UVAIB device includes an induction brazing system, a motion control system and an ultrasonic vibration system, as shown in Fig. 1. The induction brazing system is composed of an induction brazing machine, an induction coil and a gas protection device. It mainly uses the skin effect of electric current to heat the local part of the abrasive tool, so as to realize the brazing connection between CBN abrasive grains and the filler alloy. In addition, in order to prevent the filler from oxidizing, the entire induction

brazing process should be carried out under the condition of Ar gas protection. The motion control system consists of a driver, a power supply, a PLC and a motor. It mainly controls the movement of the sliding table through PLC to adjust the moving direction and speed of the induction coil. The reason why moving induction coil when brazing is that the magnetic induction line generated by the induction coil is not evenly distributed, but presents the form of dense in the middle, where generates more heat, and sparse at both ends, where generates less heat. Therefore, the heating of the grinding wheel is uneven, which leads to a large temperature gradient during brazing [29, 30]. In order to heat the abrasive tool evenly, it is necessary to control the induction coil to move while heating in order to improve the brazing quality. The ultrasonic vibration system comprises a transducer, a horn, an abrasive tool, an ultrasonic generator and a supporting structure. Through the action of the transducer and horn, electrical energy is converted into vibration mechanical energy, and then the vibration is amplified and transmitted to the abrasive tool connected to the horn through threads. At this time, the end of the abrasive tool will obtain the maximum ultrasonic amplitude. Relying on the UVAIB device, the beneficial effects of ultrasonic are used to achieve a high-quality connection between abrasive grains and filler alloy.

2.2 Experimental device and method

The filler alloy used in this study is Cu-Sn-Ti metal powder, the size of CBN abrasive grain is 40/50 mesh, the substrate material of abrasive tool is 316L stainless steel, and the ultrasonic resonance frequency is 30 kHz. The experimental setup is shown in Fig. 2. Before brazing, place the ultrasonic vibration device in the appropriate position of the sliding table and place the abrasive tool in the center of the induction coil. Subsequently, adjust the coil to an initial brazing position about 10mm below the part covered with filler. When brazing, first increase the current slowly to 7 A to preheat the grinding wheel for 80s, which is to accumulate heat for brazing. Subsequently, control the induction coil to move upward at a uniform speed of 1.5mm/s, and when it is observed that the filler alloy is completely melted, ultrasonic vibration should be applied immediately. Finally, a single-layer brazed CBN abrasive tool was obtained.

2.3 Abrasive grain shear test

The joint strength of the brazed joints was assessed by an abrasive grain shear test. As shown in Fig. 3, the abrasive tool was clamped by a cross vice, a portable microscope was used to assist in tool setting, and the abrasive grains were sheared with a cutting knife clamped by a tensile testing machine whose speed was 0.4 mm/s. A scanning electron microscope (COXEM 30) was used to observe the failure forms of brazed CBN abrasive grains after tests.

3. Structure Optimization And Performance Test Of The Uvaib Device

3.1 Structural parameter design of the UVAIB device

In the process of UVAIB, the horn plays the role of transmitting sound waves and amplifying ultrasonic vibration. Therefore, the design quality of the horn has an important impact on the performance of the

UVAIB device. Due to the limitation of the structural size of the brazing platform, an ultrasonic horn with a resonant frequency of 30kHz is developed, which can meet the requirements that the abrasive tool vibrate at the natural frequency when brazing. In addition, the horn with this simple shape machining tool as a load can be equivalent to a multi-step transition section stepped horn that is easy to calculate. A stepped horn is shown in Fig. 4a. The diameter and length of the input section and output section are D_1, D_2, and l_1, l_2, respectively. The frequency equation of the stepped horn is as follows:

$$\tan(\varphi_1 + \varphi_2) = 0 \tag{1}$$

$$\varphi_1 = k_1 l_1 \tag{2}$$

$$\varphi_2 = \arctan\left[\frac{Z_{02}}{Z_{01}}\tan(k_2 l_2)\right] \tag{3}$$

where φ_1, φ_2 is the shape factor, k is the circular wave number, $k = \omega/c$, ω is the circular frequency, $\omega = 2\pi f$, f is the resonant frequency, c is the propagation velocity of longitudinal wave in the material, $c=\sqrt{E/\rho}$, E is the elastic modulus, ρ is the density of the material, and Z is the impedance, $Z_{0n} = \rho c s_n$, s_n is the cross-sectional area of each section.

A three-step transition stepped horn is shown in Fig. 4b. The diameter and length of the input section, transition section and output section are D_1, D_2, D_3 and l_1, l_2, l_3, respectively. According to the long line theory, the stepped horn with multi-step transition section can be regarded as an acoustic transmission line, and the latter section can be regarded as the load impedance of the former section. Consequently, the frequency equation of the three-step transition stepped horn can be obtained by the recursive method as follows:

$$\tan(k_1 l_1 + \varphi_1) = 0 \tag{4}$$

$$\varphi_1 = \arctan\left[\frac{Z_{02}}{Z_{01}}\tan(k_2 l_2 + \varphi_2)\right] \tag{5}$$

$$\varphi_2 = \arctan\left[\frac{Z_{03}}{Z_{02}}\tan(k_3 l_3)\right] \tag{6}$$

$$\tan\left\{k_1 l_1 + \arctan\left[\frac{z_{02}}{z_{01}}\tan(k_2 l_2 + \arctan(\frac{z_{03}}{z_{02}}\tan(k_3 l_3))\right]\right\} = 0 \tag{7}$$

When each section of the horn is made of the same material, $k_1 = k_2 = k_3$. Based on the above equation, the size of the three-step transition stepped horn can be obtained.

3.2 Optimizing designation parameters of the UVAIB device

All components are modeled in the three-dimensional software, as shown in Fig. 5a. Subsequently, the modal analysis of UVAIB device composed of transducer, horn and abrasive tool is carried out with finite element analysis software ANSYS, and the longitudinal vibration mode is extracted, as shown in Fig. 5b. The material properties are defined in Table 1. By adjusting the length of each section of the horn, a suitable structure for the best brazing quality can be obtained. Considering the energy loss in the process of ultrasonic propagation, it is necessary to make the displacement at the connection between transition section and abrasive tool as small as possible to reduce unnecessary friction loss. As shown in Fig. 5b, the growth rate of amplitude on both sides of the last node is different, and the closer it is to the end face of the transition section, the faster the amplitude increases. Therefore, it is hoped that the position of the node is close to the end face of the transition section. That is, the value of x, which is equal to x_2 minus x_1, should be small. Where x_1 is the location of the last node, x_2 is the end face position of the transition section.

In addition, in order to study the influence of ultrasonic amplitude on brazing quality, the designed ultrasonic vibration device should have a large amplification factor M_P, which is defined as the ratio of the relative output displacement ξ_3 to the relative input displacement ξ_1, so that the amplitude can be adjusted in a large range. Furthermore, in order to obtain a higher quality brazed abrasive tool, the part of the abrasive tool covered with filler alloy should vibrate more evenly as much as possible. That is, the ratio δ of the relative vibration displacement ξ_2 at brazing starting location to the relative vibration displacement ξ_3 at the end face of abrasive tool should keep a large value.

Table 1
Material properties of the UVAIB device.

component	Material	Density ρ	Elastic modulus E	Poisson's ratio v
Horn/Wheel	316L	7930 kg/m^3	200 Gpa	0.29
Electrode sheet	Beryllium bronze		122.6 Gpa	0.35
Front/rear cover plate	6061Al	8250 kg/m^3	72 Gpa	0.33
Piezoelectric ceramics sheet	Piezoelectric ceramics	2750 kg/m^3	68 Gpa	0.3
		7600 kg/m^3		

In practice, the size of D_1 is determined by the transducer end face and the size of D_3 and l_3 is determined by the abrasive tool. Therefore, considering the influence of transition section diameter on the performance of horn, the different D_2 are taken for calculation and the corresponding values of l_1 and l_2 can be obtained. According to the calculation results, the relationship between the length of l_2 and l_1 is

shown in Fig. 6a. When the length of l_2 increases from 20 mm to 90 mm, the length of l_1 shows a downward trend. In addition, in the range of 20 mm to 60 mm, the larger the value of D_2, the faster the length of l_1 will drop. However, when the length of l_2 is in the range of 60 mm to 90 mm, the length of l_1 tends to be the same for different D_2. After modeling with above values and carrying out the modal analysis, the effect of length of l_2 on the relative distance of node is obtained, as shown in Fig. 6b. When the length of l_2 increases from 20 mm to 40 mm, the relative distance of node keeps decreasing. When the length of l_2 is in the range of 40 mm to 60 mm, the relative distance of the node tends to be stable, which fluctuates only in a small range. After the length of l_2 reaches 60 mm, the relative distance of the node generally becomes an upward trend. Especially from the overall trend, when the value of D_2 increases, the relative distance of the node will also increase. Therefore, in order to obtain a small relative distance of the node, the length of l_2 should be in the range of 40 mm to 60 mm.

As a result, the amplification factor is studied under the above restrictions. As shown in Fig. 6c, when the length of l_2 increases from 40 mm to 60 mm, the amplification factor for different D_2 shows a straight upward trend. In addition, as the value of D_2 increases, the corresponding amplification factor also increases. Therefore, for the consideration of obtaining a large amplification factor, the length of l_2 is decided to be 60 mm. Besides, combined with Fig. 5b, in order to obtain a small relative distance of the node and a large amplification factor simultaneously, the value of D_2 should be 19 mm.

It is known that when the length of l_2 is 60 mm, the corresponding length of l_1 is about 80 mm. Thus, in order to obtain a higher vibration uniformity, the influence of length of l_1 on the vibration uniformity is studied, which is in the range of 76 mm to 84 mm. As shown in Fig. 6d, when the length of l_1 increases from 76 mm to 84 mm, the vibration uniformity first decreases and then increases. When the length of l_1 is 80 mm, the vibration uniformity of the UVAIB device is 92%, which is the highest value. Subsequently, the value of vibration uniformity shows a downward trend. Therefore, the length of l_1 is determined to be 80 mm.

In summary, the size of the horn is determined as D_2 = 19 mm, l_1 = 80 mm and l_2 = 60 mm. The simulation results indicate that the resonant frequency of the ultrasonic vibration device is 30171 Hz, and after setting the flange, the resonant frequency becomes 30243 Hz, as shown in Fig. 7. At this time, the ultrasonic energy loss can be reduced, the amplification factor can reach 8, and the vibration uniformity of abrasive tools can reach 92%.

3.3 Performance test on the UVAIB device

3.3.1 Impedance analysis test

The horn is manufactured with the optimized size and assembled with transducer and abrasive tool to form an ultrasonic vibration device. The impedance characteristics are analyzed by the PV502A impedance analyzer and the analysis results are shown in Fig. 8. There is no parasitic circle in the

admittance circle diagram and the impedance-frequency curve is relatively smooth, which indicates that the vibration near the resonance point is ideal. In addition, the dynamic resistance is 38.76 Ω, which shows that the ultrasonic vibration device has high energy utilization during working. The mechanical quality factor is reasonable, which indicates that the conversion efficiency of electric energy and sound energy is high.

From the overall results, there is a difference between the actual value (f = 30653Hz) and the theoretical value (f = 30243Hz) of the resonant frequency, because the material characteristic value is not exactly the same as the defined value of modal analysis. In addition, the horn and the abrasive tool are connected through threads, so the gap generated in the assembly process also causes errors. In short, the structure of the horn is reasonable and the ultrasonic vibration device has good ultrasonic performance.

3.3.2 Amplitude test

Ultrasonic amplitude is one of the key factors affecting the quality of UVAIB. In this text, a laser doppler vibrometer (LV-S01, SOPTOP) was used to measure the ultrasonic amplitude. Five points with the same interval on the end face of abrasive tool are measured for 3 times and the average value was taken as the amplitude of the vibration device, which is measured to be 5 μm, as shown in Fig. 9. The peak value of the waveform corresponds to the ultrasonic amplitude and it is found that the longitudinal vibration curve is approximately sinusoidal, which indicates that the ultrasonic vibration device has good ultrasonic performance.

4 Effect Of Ultrasonic Acoustic Effect On Brazed Cbn Joints

4.1 Surface morphology of the brazed CBN joints

For CIB, the surface of filler alloy is uneven and contains a large number of pores and small pits, as shown in Figs. 10a and 10b. However, the UVAIB filler alloy is spread more evenly and there are a few pores and almost no pits, as shown in Figs. 10c and 10d. In addition, the number of pores was counted by image processing software, as shown in Fig. 11. It is found that the pore diameter of two methods is both concentrated in 3–9 μm. Meanwhile, compared with CIB, the number of pores of UVAIB is greatly reduced and the pore diameter is smaller.

Figure 12 vividly illustrates the formation process of pores for CIB. In this study, the abrasive grains are adhered to the substrate through the adhesive, and then paved with a layer of filler alloy evenly. Therefore, when the abrasive tool is heated, the adhesive will volatilize and produce a large amount of gas, which needs to go a certain distance in the liquid filler alloy to separate. However, due to the fast heating speed and relatively short heating time in the induction heating process, the volatilized gas does not have enough time to discharge. In addition, the cooling rate after brazing is also fast, so a considerable part of the gas fails to separate from the filler alloy before solidification, which results in a fact that a large number of pores will be formed inside and on the surface of the filler alloy.

Besides, the filler alloy is a blend of different metal powders. Although it is dispersed by physical vibration before distributing on the substrate of abrasive tool, some filler alloy is still agglomerated together, which will make the filler layer loose and empty when brazing. Meanwhile, the filler alloy is manually sprayed on the surface of abrasive tool layer by layer, which is impossible to ensure the uniformity of filler layer thickness and will lead to hollow structures of filler layer. Therefore, these factors will inevitably lead to pits and roughness on the filler surface after brazing.

However, the surface morphology of UVAIB joints remains in good condition. The obvious difference can be attributed to the ultrasonic oscillatory motion, acoustic streaming effect and cavitation effect. As shown in Figs. 12 and 13, under the action of ultrasonic oscillation, the mixing and flow of filler alloy are enhanced, which makes the filler alloy tend to be uniform and flat. In addition, ultrasonic oscillation motion is also conducive to gas escape. At the same time, the acoustic streaming effect also has a beneficial effect on the brazing process. When ultrasonic propagates in the liquid filler alloy, due to the absorption and attenuation of sound wave, it will form a sound pressure gradient from the sound source to its propagation direction, which will promote the flow of liquid filler. Furthermore, when the amplitude of ultrasonic vibration increases to a certain value, this non-periodic movement will produce a fluid jet phenomenon in the filler, and its flow speed is greater than that generated by the thermal convection inside the liquid filler. Therefore, the acoustic streaming effect can speed up the flow of liquid filler, which not only makes the pores reduce but also makes the filler layer flat, as shown in Figs. 12 and 13.

In addition, when ultrasonic vibration acts in the liquid filler alloy, the tiny bubbles in the filler will be stretched and become cavitation bubbles. Subsequently, these cavitation bubbles will collapse under pressure. During this process, an instantaneous high temperature and high pressure environment was produced in local areas, which is shown as a strong shock different from the macro vibration. Moreover, the high temperature, high pressure and micro jet caused by ultrasonic cavitation will produce many local reactions in the liquid filler, which can promote the chemical metallurgical reaction of brazing. At the same time, the collapse of the cavitation bubble can realize the stirring of the liquid filler alloy. Therefore, the gas in it can escape more easily.

4.2 Physical property of brazed CBN joints

4.2.1 Cracks on brazed CBN joints

The cracks of CIB and UVAIB joints are compared in Fig. 14. For CIB, it can be found that long and wide macro-cracks distribute on the bond zone, as shown in Figs. 14a and 14b. However, only fewer and smaller micro-cracks are found on the joints of UVAIB, as shown in Figs. 14c and 14d. It is known that the brittle CBN abrasive grains, plastic Cu-Sn-Ti filler alloy and stainless-steel substrate of abrasive tool have a difference in thermal expansion coefficient, which will cause the mismatch of connecting components. Therefore, the brazed CBN abrasive grains will appear the thermal damage after brazing, which may cause cracks on the grains. Moreover, due to uneven temperature changes, thermal residual stress will be generated during brazing. These factors lead to the existence of many macro-cracks on the CIB joints,

which will inevitably reduce the strength and wear resistance of the grains. However, for UVAIB, since the ultrasonic oscillation motion and the acoustic streaming effect can accelerate the heat transfer of molten filler alloy and make the brazing temperature more uniform, the degree of thermal damage and thermal residual stress can be alleviated. Therefore, there are fewer and smaller micro-cracks on the brazed joints.

4.2.2 Fracture forms of brazed CBN abrasive grains

After the abrasive grain shear test, the fracture forms of abrasive grains are compared in Fig. 15. It is found that the abrasive grains of CIB fail in the form of intergranular fracture. Many pores are found at the interface between abrasive grains and filler alloy, as shown in Fig. 15a. While the abrasive grains of UVAIB fail in the form of transgranular fracture, as shown in Fig. 15b. It is found that the bonding interface remains in good condition. The evolution process of abrasive grains failure is shown in Fig. 16. For CIB, when the abrasive grains are subjected to a shear force, the cracks will first appear at the location of pores in the filler alloy. This is because these pores are places of stress concentration, which will easily become crack initiation. When the shear force increases, these micro-cracks will grow into macro-cracks and filler alloy will lose control of abrasive grains. Finally, the abrasive grains fail in the form of intergranular fracture. Therefore, the existence of pores will weaken the holding force of filler alloy on abrasive grains.

For UVAIB, on the one hand, there are a few pores on joints. Therefore, the holding force will be basically unaffected. When the shear force increases, the micro-cracks will first appear on the grains and then expand into macro-cracks. Finally, the abrasive grains fail in the form of transgranular fracture, as shown in Fig. 16, which indicates that the holding force of filler alloy on abrasive grains exceeds the fracture strength of abrasive grains. On the other hand, the cavitation effect will occur at the capillary gap in the liquid filler alloy. The generation, growth and collapse of these cavitation bubbles will produce large local pressure and strong ultrasonic impact, which can break the precipitated phase and make large grains into small pieces. Meanwhile, these small pieces become new nucleation centers that will promote the growth of new grains. Therefore, ultrasonic vibration refines the grains, which can optimize the brazing structure and improve the holding force of filler alloy on CBN abrasive grains.

5. Conclusion

In this paper, through the combination of theory and simulation, an UVAIB device is developed for the manufacture of brazed CBN abrasive tool, and the advantages of ultrasonic vibration in improving brazing quality have been verified by UVAIB experiment. The following conclusions are drawn:

1. An UVAIB device is developed, and the longitudinal ultrasonic vibration with an amplitude of 5 μm is achieved on the end of abrasive tool. The amplification factor and vibration uniformity of the abrasive tool are the key factors in the design of the ultrasonic vibration device. In this work, the ultrasonic energy loss of the UVAIB device could be reduced, and then the amplification factor value and vibration uniformity could reach 8 and 92%, respectively.

2. For CIB, the surface of the filler alloy is uneven and there are a large number of pores and macro-cracks on the joints. However, the UVAIB filler alloy is spread more evenly. The internal pores inside the metallic matrix were reduced, and only fewer and smaller micro-cracks were found.

3. The abrasive grains of CIB failed in the form of intergranular fracture, while those of UVAIB failed in the form of transgranular fracture, which could be attributed to the stronger bonding strength of UVAIB joints compared with CIB. These beneficial effects are due to the work of ultrasonic oscillation motion, acoustic streaming effect and cavitation effect.

Declarations

Funding This work was financially supported by the National Natural Science Foundation of China (Nos. 51921003, 92160301 and 52175415), Natural Science Foundation of Jiangsu Province (No. BK20210295), the Open Foundation State Key Laboratory of Mechanical Transmissions (No. SKLMT-MSKFKT-202101), and the Postgraduate Research & Practice Innovation Program of Jiangsu Province (No. SJCX21-0106).

Competing interests The authors have no conflicts of interest to declare that they are relevant to the content of this article.

Availability of data and material All data generated or analyzed during this study are included in the present article.

Authors' contributions Kaida Cai: experimentation, data curation, and writing the original draft. Biao Zhao: data collection and manuscript revision. Bangfu Wu: experimentation and methodology. Wenfeng Ding: supervision, conceptualization, and methodology.

Ethics approval and consent to participate The article follows the guidelines of the Committee on Publication Ethics (COPE) and involves no studies on human or animal subjects.

Consent to participate Not applicable.

Consent for publication Not applicable.

References

1. Xiao HZ, Wang SY, Xiao B (2022) Microstructural characteristics and mechanical properties of diamond grinding wheel brazed with modified Ni-Cr-W alloy using continuous tunnel furnace. Ceram Int 48:9258–9268

2. Mukhopadhyay P, Ghosh A (2022) The making and performance of patterned-monolayer brazed diamond wheel produced with Ag-based novel active filler. J Manuf Process 73:220–234
3. Zhang L (2021) Filler metals, brazing processing and reliability for diamond tools brazing: A review. J Manuf Process 66:651–668
4. Li QL, Ding K, Lei WN et al (2021) Investigation on induction brazing of profiled cBN wheel for grinding of Ti-6Al-4V. Chin J Aeronaut 34:132–139
5. Zhao B, Ding WF, Xiao GD et al (2022) Self-sharpening property of porous metal-bonded aggregated cBN wheels during the grinding of Ti–6Al–4V alloys. Ceram Int 48:1715–1722
6. Wu SX, Zhang FL, Ni YQ et al (2020) Grinding of alumina ceramic with microtextured brazed diamond end grinding wheels. Ceram Int 46:19767–19784
7. Wu QP, Ouyang ZY, Wang Y et al (2019) Precision grinding of engineering ceramic based on the electrolytic dressing of a multi-layer brazed diamond wheel. Diam Relat Mater 100:107552
8. Ghosh A, Chattopadhyay AK (2007) On grain-failure of an indigenously developed single layer brazed CBN wheel. Ind Diamond Rev 1:59–64
9. Ding WF, Xu JH, Chen ZZ et al (2013) Interface characteristics and fracture behavior of brazed polycrystalline CBN grains using Cu–Sn–Ti alloy. Mater Sci Eng A 559:629–634
10. Mukhopadhyay P, Simhan DR, Ghosh A (2017) Challenges in brazing large synthetic diamond grit by Ni-based filler alloy. J Mater Process Technol 250:390–400
11. Li HB, Chen T, Duan ZY et al (2022) A grinding force model in two-dimensional ultrasonic-assisted grinding of silicon carbide. J Mater Process Technol 304:117568
12. Chen Y, Hu ZW, Yu YQ et al (2022) Processing and machining mechanism of ultrasonic vibration-assisted grinding on sapphire. Mater Sci Semiconduct Process 142:106470
13. Wen J, Tang JY, Zhou WH (2022) Study on formation mechanism and regularity of residual stress in ultrasonic vibration grinding of high strength alloy steel. J Manuf Process 66:608–622
14. Zhang P, Zhang XC, Cao X et al (2021) Analysis on the tool wear behavior of 7050-T7451 aluminum alloy under ultrasonic elliptical vibration cutting. Wear 466:203538
15. Airao J, Nirala CK (2022) Machinability of Ti-6Al-4V and Nimonic-90 in ultrasonic-assisted turning under sustainable cutting fluid. *Materials Today: Proceedings, 10.1016/j*i>.matpr.2022.02.312.
16. Peng ZL, Zhang XY, Zhang DY (2021) Effect of radial high-speed ultrasonic vibration cutting on machining performance during finish turning of hardened steel. Ultrasonics 111:106340
17. Yang HL, Wang JJ, Zhang JF et al (2021) On the material removal mechanism in rotary ultrasonic milling of ultralow-density silica aerogel composites. J Manuf Process 70:621–635
18. Chen GJ, Xu JK, Wang JD et al (2022) Numerical and experimental study on the amplitude effect of ultrasonic vibration-assisted milling of 3D needle-punched Cf/SiC composite. Ceram Int 48:17893–17914
19. Cao Y, Zhu YJ, Li HN et al (2020) Development and performance of a novel ultrasonic vibration plate sonotrode for grinding. J Manuf Process 57:174–186

20. Zhao B, Chang BQ, Wang XB et al (2019) System design and experimental research on ultrasonic assisted elliptical vibration grinding of Nano-ZrO2 ceramics. Ceram Int 45:24865–24877
21. Bai W, Wang K, Du DX et al (2022) Design of an ultrasonic elliptical vibration device with two stationary points for ultra-precision cutting. Ultrasonics 120:106662
22. Du PF, Han L, Qiu X et al (2022) Development of a high-precision piezoelectric ultrasonic milling tool using longitudinal-bending hybrid transducer. Int J Mech Sci 222:107239
23. Wu KL, Yuan XJ, Li T et al (2019) Effect of ultrasonic vibration on TIG welding–brazing joining of aluminum alloy to steel. J Mater Process Technol 266:230–238
24. Nie Y, Zhu L, Lang Q et al (2022) Ultra-rapid and low-temperature soldering of hypereutectic Al-Si alloys by ultrasonic-assisted soldering with In interlayer in air for electronic application.Journal of Advanced Joining Processes100115
25. Cui W, Li SQ, Yan JC et al (2015) Ultrasonic-assisted brazing of sapphire with high strength Al-4.5Cu-1.5Mg alloy. Ceram Int 41:8014–8022
26. Zhang CG, Ji HJ, Xu HB et al (2020) Interfacial microstructure and mechanical properties of ultrasonic-assisted brazing joints between Ti–6Al–4V and ZrO_2. Ceram Int 46:7733–7740
27. Chen XG, Yan JC, Ren SH et al (2014) Microstructure, mechanical properties, and bonding mechanism of ultrasonic-assisted brazed joints of SiC ceramics with ZnAlMg filler metals in air. Ceram Int 40:683–689
28. Huang GQ, Huang JR, Zhang MQ et al (2018) Fundamental aspects of ultrasonic assisted induction brazing of diamond onto 1045 steel. J Mater Process Technol 260:123–136
29. Lu LL, Zhang SM, Xu J et al (2017) Numerical study of titanium melting by high frequency inductive heating. Int J Heat Mass Transf 108:2021–2028
30. Kranjc M, Zupanic A, Miklavcic D et al (2010) Numerical analysis and thermographic investigation of induction heating. Int J Heat Mass Transf 53:3585–3591

Figures

Figure 1

Schematic diagram of the UVAIB device.

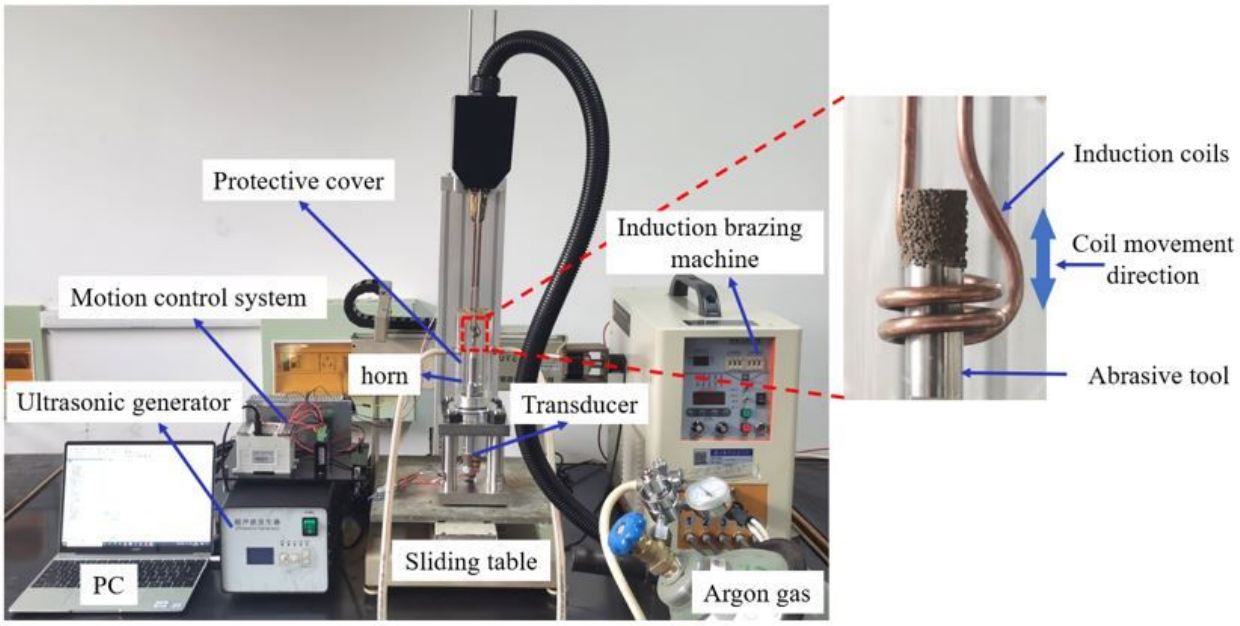

Figure 2

UVAIB experimental setup.

Figure 3

Abrasive grain shear test: (a) relevant devices, (b) illustration of shearing.

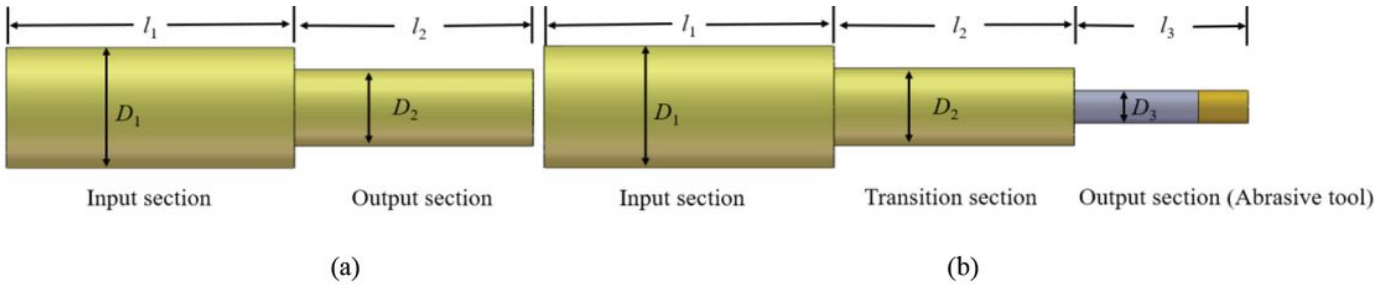

Figure 4

Geometry of the horn: (a) stepped horn (b) three-step transition stepped horn.

Figure 5

Modal analysis: (a) Model of the ultrasonic vibration device, (b) Relative displacement distribution of the horn.

Figure 6

(a) Relationship between length of l2 and l1 for different D2, (b) Effect of length of l2 on relative distance of node for different D2, (c) Effect of length of l2 on amplification factor for different D2, (d) Effect of length of l1 on vibration uniformity.

Figure 7

Modal analysis results of the ultrasonic vibration device.

Figure 8

Impedance analysis device and results.

Figure 9

Amplitude test device and results.

Figure 10

Surface morphology of the filler alloy: (a)(b) CIB, (c)(d) UVAIB.

Figure 11

Pore statistics: (a) Number of pores with different diameters, (b) Distribution of pores with different diameters.

Figure 12

Schematic diagram of pores formation during brazing.

Figure 13

Schematic diagram of the influence of ultrasonic vibration on brazed joints.

Figure 14

Cracks on brazed joints: (a)(b) CIB, (c)(d) UVAIB.

Figure 15

Fracture forms of brazed CBN abrasive grains: (a) CIB, (b) UVAIB.

Figure 16

Schematic diagram of the evolution process of CBN abrasive grain shear morphology.